International Journal of Nanomedicine

Dovepress
open access to scientific and medical research

Open Access Full Text Article

ORIGINAL RESEARCH

Intelligent Drug Delivery Microparticles with Visual Stimuli-Responsive Structural Color Changes

This article was published in the following Dove Press journal:
International Journal of Nanomedicine

Xiaoyan Sun
Lingzi Liu
Hui Zou
Caixia Yao
Zhengyu Yan
Baofen Ye

Key Laboratory of Biomedical Functional Materials, School of Science, China Pharmaceutical University, Nanjing, Jiangsu 210009, People's Republic of China

Background: Particle-based drug delivery systems (DDSs) have a demonstrated value for drug discovery and development. However, some problems remain to be solved, such as limited stimuli, visual-monitoring.

Aim: To develop an intelligent multicolor DDSs with both near-infrared (NIR) controlled release and macroscopic color changes.

Materials and Methods: Microparticles comprising GO/pNIPAM/PEGDA composite hydrogel inverse opal scaffolds, with dextran and calcium alginate hydrogel were synthesized using SCCBs as the template. The morphology of microparticle was observed under scanning electron microscopy, and FITC-dextran-derived green fluorescence images were determined using a confocal laser scanning microscope. During the drug release, FITC-dextran-derived green fluorescence images were captured using fluorescent inverted microscope. The relationship between the power of NIR and the drug release rate was obtained using the change in optical density (OD) values. Finally, the amount of drug released could be estimated quantitatively used the structural color or the reflection peak position.

Results: A fixed concentration 8% (v/v) of PEGDA and 4mg/mL of GO was chosen as the optimal concentration based on the balance between appropriate volume shrinkage and structure color. The FITC-dextran was uniformly encapsulated in the particles by using 0.2 wt% sodium alginate. The microcarriers shrank because of the photothermal response and the intrinsic fluorescence intensity of FITC-dextran in the microparticles gradually decreased at the same time, indicating drug release. With an increasing duration of NIR irradiation, the microparticles gradually shrank, the reflection peak shifted toward blue and the structural color changed from red to orange, yellow, green, cyan, and blue successively. The drug release quantity can be predicted by the structural color of microparticles.

Conclusion: The multicolor microparticles have great potential in drug delivery systems because of its vivid reporting color, excellent photothermal effect, and the good stimuli responsivity.

Keywords: drug delivery, microparticles, color change, graphene oxide, photothermal effect

Introduction

Drug delivery systems (DDSs) have received significant attention because of their superior performance in controlled-release of many drugs to treat diseases.[1–7] The controlled release behavior and targeted-delivery capability of DDSs greatly increase the therapeutic efficiency and reduce the side effects.[8–17] Microparticle DDSs are an interesting and promising option that can incorporate different types of biodegradable and biocompatible polymer components, endowing them with features such as high efficiency, good stability, low side effects and easy modification.[18,19] Different stimuli have been used as control switches, such as

Correspondence: Baofen Ye
Key Laboratory of Biomedical Functional Materials, School of Science, China Pharmaceutical University, Nanjing, Jiangsu 210009, People's Republic of China
Tel +86 13951725591
Email baofen_ye@163.com

submit your manuscript | www.dovepress.com
DovePress
http://doi.org/10.2147/IJN.S249009

pH,[20,21] temperature,[22,23] light,[24] magnetism,[25,26] and electricity.[27] As one of the important stimuli, light is considered an ideal source for photo-mediated cancer therapy such as photo-thermal or photo-dynamic therapy. Near-infrared (NIR) light which can reduce body tissue damage and enhance tissue penetration has become an attractive stimulus.[28] Graphene oxide (GO) has been widely used in Photodynamic therapy because of its excellent photothermal effect, good biocompatibility and low manufacturing cost.[29–36] To date, most GO-mediated DDSs have been limited to particles with relatively simple structures and poor drug release for macromolecular drugs.[37] Inspired by inverse opal structures, much effort has been made toward the construction of porous stimuli-responsive structural color materials.[38,39] In contrast to traditional stimuli-responsive DDSs, stimuli-responsive DDSs with hybrid inverse opal structures provide abundant interior pores and large specific surface areas for drug loading.[40–46] In addition, inverse opal structure microparticles have optical properties and the swelling or contraction of the microparticles will result in Bragg diffraction peak shifts.[47,48] Zhang et al designed a poly (N-isopropylacrylamide) (pNIPAM) inverse opal hydrogel particles that showed controllable release triggered by temperature.[49] The characteristic reflection peak allowed real-time monitoring of drug release from the particles. Liu et al designed hybrid inverse opal structured egg microparticles with for synergistic drug delivery.[50] Although remarkable progress has been made in this area, some problems remain to be solved, such as limited stimuli and visual-monitoring. In the present study paper, we developed a novel drug delivery system with both NIR controlled release and macroscopic color changes as a reporting signal for drug release. The inverse opal microparticles comprised pNIPAM, poly (ethylene glycol) diacrylate (PEGDA), and GO. PNIPAM hydrogels have received increased research attention as thermo-responsive hydrogels because of its good biocompatibility and swelling property, which transit approximately at body temperature. PEGDA was used as a comonomer to enhance the structural color of the inverse opals. The NIR heating characteristic of GO and the temperature sensitivity of the pNIPAM hydrogel scaffold meant that the inverse opal microparticles shrank under NIR illumination, which squeezed the encapsulated drugs out of the particles. During this process, the microparticle's color changed correspondingly. Therefore, the color of the microparticles could be used as a signal to monitor and quantify drug release. Thus, these features of the self-reporting inverse opal microparticles make them ideal for external drug delivery applications such as wound surgical dressing materials.

Materials and Methods

Materials

Nanjing Nanorainbow Biotechnology Co., Ltd. (Nanjing, China) provided the SiO2 nanoparticles at sizes of 250 and 215 nm. Aladdin Industrial Corporation (Shanghai, China) provided poly (ethylene glycol) diacrylate (PEGDA, average molecular weight,700), N-isopropylacrylamide (NIPAM, 97%), calcium chloride, sodium alginate, and hydrofluoric acid. The GO suspension was purchased from XF NANO (Nanjing, China). Fluorescein isothiocyanate-dextran (FITC-dextran, average molecular weight, 150,000) was purchased from Sigma-Aldrich (St. Louis, MO, USA). All other chemicals and reagents were acquired at the best grade available and were used as received.

Template Colloidal Crystal Beads Generation

The microfluidic droplet template method was used to generate the silica colloidal crystal beads (SCCBs). The aqueous suspension of SCCBs and hexadecane with 0.05% surfactant 2296 were pumped into a single emulsion microfluidic device. In the microfluidic channel, hexadecane sheared the aqueous suspension into droplets. The silica nanoparticles were used at a concentration of 15% wt. The injection speed of the oil phase was 15 mL/h and that of the dispersed phase was 40 mL/h. A plastic container filled with hexadecane was used to collect the resultant droplets. Then, evaporation at 60°C in an oven over 24 h allowed the silica nanoparticles in the droplets to self-assemble into ordered lattices. Finally, calcination at 800°C for 3 h was used to improve the mechanical strength of the SCCBs.

Fabrication of Thermo-Responsive Inverse Opal Microparticles

A pre-gel solution containing NIPAM, PEGDA, GO (at different concentrations), and HMPP (1% v/v) was used to fabricate the thermo-responsive inverse opal particles. The SCCBs were pretreated with piranha solution (30% v/v hydrogen peroxide and 70% v/v sulfuric acid) for 6 h to ensure that the pre-gel solution could entirely fill the void.

The SCCBs were washed with water, dried in a vacuum dryer, and immersed in the pre-gel solution for 1 h. Exposure to UV light for 10 seconds was then used to polymerizate the pre-gel solution inside and outside of the SCCBs. Finally, the silica template was removed by immersion in hydrofluoric acid (3%, v/v) for 2 h to obtain the thermo-responsive inverse opal microparticles. Photographs, microstructure images, and the reflection spectra of the inverse opal particles were then obtained.

Characterization

A light microscope (OLYMPUS BX51, Tokyo, Japan) equipped with a color CCD camera (Media Cybernetics Evolution MP 5.0, Media Cybernetics, Rockville, MD, USA) was used to take photographs of the SCCBs. An Ideaoptics Instruments FX4000 reflection spectrometer (200–1100 nm; Ideaoptics Instruments, London, UK) recorded the reflection spectra. Scanning electron microscopy (SEM, ZEISS, ULTRA 55; Carl Zeiss, Jena, Germany) was used to characterize the microparticles' microstructures. A confocal laser scanning microscope (CLSM, LSM800, Zeiss) was used to acquire fluorescent images, which were processed using the ZEN imaging software.

Drug Loading and Encapsulation

FITC-dextran is one of the hydrophilic drugs. Sodium alginate pre-gel solutions of various concentrations (0.2, 0.4, 0.6, 0.8, and 1.0% (w/v)) were prepared and mixed with 2.0 mg/mL FITC-dextran. Inverse opal particles, which had a characteristic reflection of 650 nm, were incubated in the mixture for more than 2 h. Then, to produce a calcium alginate hydrogel, 2.0% (w/v) calcium chloride was added to the mixture. It was not possible to quantify the drug content of each microcarrier using ultraviolet spectrophotometry because a dozen or even dozens of microcarriers are simultaneously immersed in the drug during the drug embedding process. A microscope (OLYMPUS IX71) with a high-resolution CCD camera (OLYMPUS DP72) was then used to acquire images of the inverse opal microparticles. The OD values of FITC-dextran of the microparticles were then calculated using Image J software (NIH, Bethesda, MD, USA) based on the fluorescent images.[49,50] A CLSM (LSM700, Zeiss) was then used to acquire fluorescence cross-sectional images, which were processed using the ZEN imaging software.

In vitro Controlled Drug Release and Monitoring

The release kinetics of the drug-loaded microparticles were investigated by irradiating the inverse opals using NIR in phosphate-buffered saline (PBS, pH=7.4) as the release medium. A microscope (OLYMPUS IX71) captured images of the green fluorescence of the microparticles using a high-resolution CCD camera (OLYMPUS DP72) each minute after NIR irradiation at different powers. The OD values of the microparticles was then calculated using image J software. Finally, we obtained the relationship between the power of NIR and the drug release rate using the change in OD values.

Results and Discussion

Typically, the microfluidic device-generated droplet templates were used to prepare SCCBs by self-assembly into nanoparticles. During the evaporation of the solvents, the silica nanoparticles formed a closely packed hexagonal structure in the bead templates. Immersion of the spherical colloidal crystal templates in the pregel solution allowed the pregel solution to penetrate into the voids between the nanoparticles under capillary force. Subsequent exposure of the mixture to UV light polymerized the pregel solution in and around the templates. The inverse opal hydrogel particles were then obtained by removing the hydrogel outside the colloidal crystal templates and etching the silica nanoparticles in the templates.

The inverse opal hydrogel particle scaffold mainly comprised N,N'-methylenebis-(acrylamide) (BIS), NIPAM, PEGDA, and GO. To impart a bright stimuli-responsive color function to the particles, the high refractive index comonomer, PEGDA, was incorporated into the pregel solution via copolymerization. This not only improved the hydrogel particles' mechanical strength, but also enhanced the carrier's reflective color, such that it could be observed by the naked eye (Figure S1). An investigation of the effect of the PEGDA concentration on the volume shrinkage of the inverse opals showed that a high PEGDA concentration enhanced the bright color of the inverse opals. However, it also reduced the volumetric shrinkage (Figure S2a). After comprehensive consideration of the color and volumetric shrinkage, we chose a PEGDA concentration of 8% (v/v). At this concentration, the inverse opal hydrogel particles showed a good swelling capacity and a bright color. GO was physically doped in the three-dimensional network of pNIPAM-PEGDA hydrogel. The hydrogen–bond interaction between hydrogel network and GO sheets large enough that it would not leak out of the

hydrogel network. The appropriate concentration of GO was also studied to achieve a good photothermal heating effect. GO at a relatively high concentration of 5 mg/mL inhibited polymerization of the composite hydrogel. However, GO at 1 mg/mL displayed a low NIR absorption. They both decreased the volume shrinkage of the composite hydrogel (Figure S2b). Therefore, 4 mg/mL GO was used. Under this optimized GO concentration, we achieved the best photothermal conversion efficiency and the best response of our hydrogel.

The SCCB templates and their derived inverse opal microparticles had orderly arranged nanostructures that had unique photonic band gaps (PBGs), which prevented the propagation of light at certain wavelengths inside the crystal structure. This resulted in the SCCB templates and derived inverse opal particles having characteristic reflection peaks and vivid colors (Figure 1). Using different sizes of SiO2 nanoparticles, microparticles with different structural colors could be obtained.

The template SCCBs and the inverse opal microparticles' microstructures were characterized using SEM (Figure 2). The silica nanoparticles on the SCCB surface were arranged hexagonally (Figure 2A and B), and this structure extended to the inside of the beads (Figure 2C). This suggested that the pNIPAM hydrogel particles formed using the SCCB templates would have a similar highly ordered inverse opal structure, together with interconnected pores. The relatively low concentrations and cross-linking degrees of the hydrogel scaffolds of inverse opal microparticles meant that they tended to shrink and collapse during drying (Figure S3). Therefore, during drying, a high concentration of the PEGDA hydrogel (100% v/v) was used to maintain the nanostructure to further investigate the actual nanostructure of the replicated microparticles. Figure 2D shows that the replicated hydrogel particles possessed a hexagonal symmetrical porous surface. The pores were also interconnected (Figure 2E and F). This porous interconnected inverse opal nanostructure represented a method for active drug loading and release.

The inverse opal microparticles were exposed to NIR light to confirm their equation below, the center-to-center distance between two neighboring nanopores decreases, resulting in a blue shift in the reflected wavelength of microcarriers. Under NIR irradiation, the microparticles shrank and their color changed from red to orange, yellow, green, cyan, and blue successively (Figure 3). This could be attributed to the photoexcitation effect of GO, which generated local heat, thereby warming the hydrogel. When the temperature increased beyond the lower critical solution temperature of pNIPAM, the hydrogel would shift from its hydrophilic state

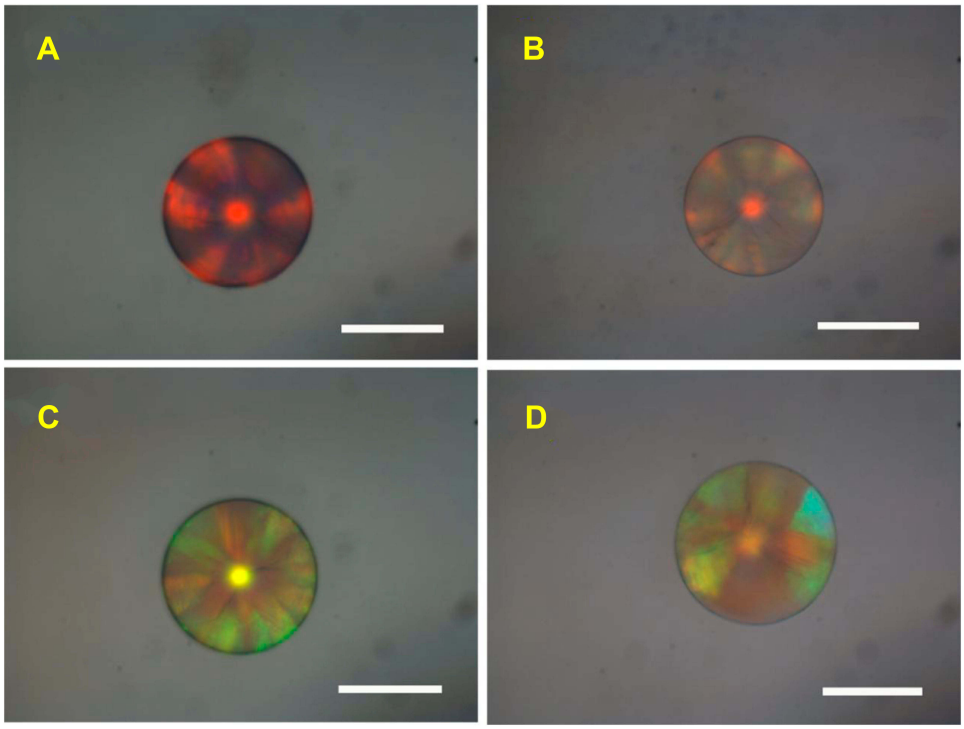

Figure 1 The reflection images of two different colored microparticles: (**A**–**C**) Silica colloidal crystal beads (SCCBs) prepared by silica nanoparticles with 250 nm (top) and 215 nm (bottom), respectively. (**B** and **D**) Inverse opal microparticles with 8% (v/v) poly (ethylene glycol) diacrylate (PEGDA) and 4 mg/mL graphene oxide (replicated from a and c, respectively). Scale bars = 50 μm.

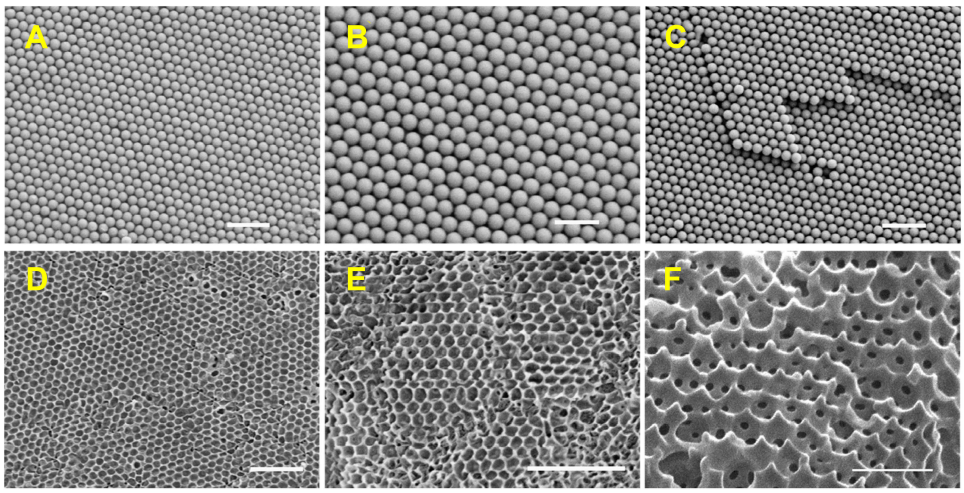

Figure 2 Different kinds of microparticles viewed under a scanning electron microscope: (**A**–**C**) The surface microstructures (**A** and **B**) and the interior (**C**) of the template. (**D**–**F**) the surface microstructures (**D**) and interior (**E** and **F**) of the inverse opal microcarriers. Scale bars are 1 μm (**A**), 200 nm (**B**), 1 μm (**C**), 500 nm (**D**), 1 μm (**E**), and 1 μm (**F**).

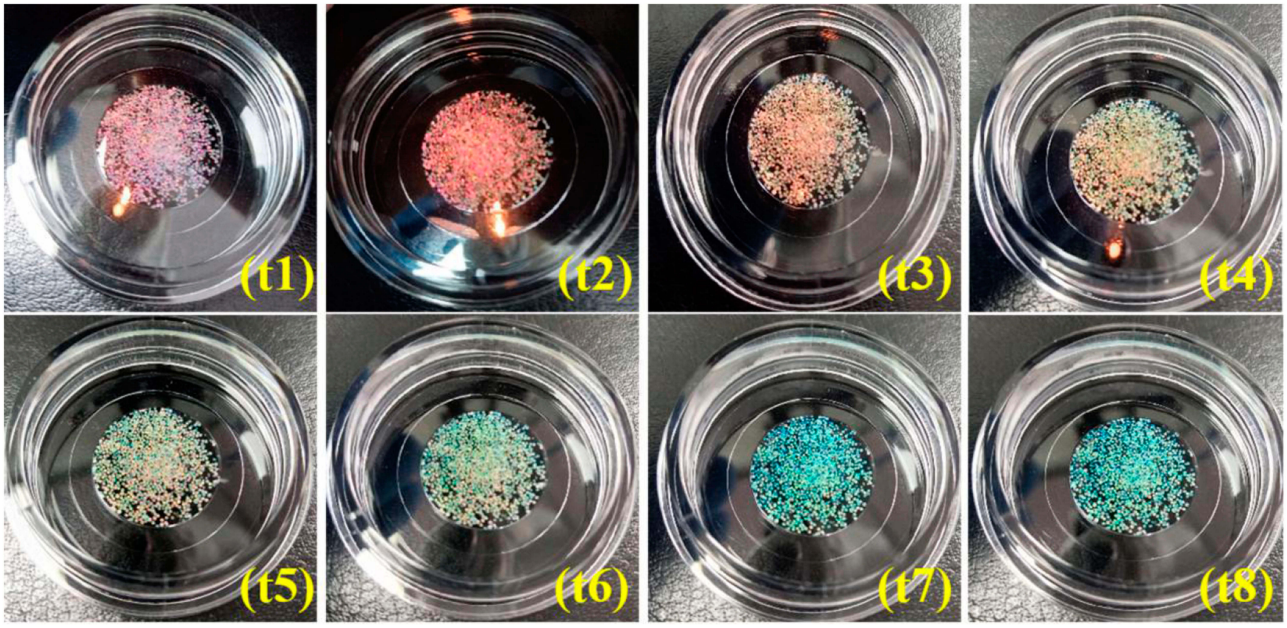

Figure 3 The color change reflection images of the microcarriers every 1 min under near-infrared (NIR) light: (t1–t8) microcarriers that shrank under NIR irradiation and their structural color changed from red to orange, yellow, green, cyan, and blue successively.

to a hydrophobic state and the microparticles appeared to shrink. The microparticles swelled and the color gradually returned to red when the NIR source was turned off. This transition could be repeated successfully over 20 times and the microparticles showed good durability (Figure S4). Dextran is a water-soluble macromolecular polysaccharide polymer drug. The pore size of the inverse opal microcarriers we prepared was more than 200 nanometers; therefore, FITC-dextran was then chosen as a macromolecular model drug for loading and controlled release in a proof of the concept for particle-based drug delivery experiment. We used a second calcium alginate hydrogel to encapsulate the drug in the microcarriers. The pregel solution containing 0.2 wt% sodium alginate was first used to dissolve FITC-dextran. The mixed solution was then allowed to infiltrate the pores of the inverse opal hydrogel microparticles. Finally, the mixed solution was polymerized and the drug-loaded inverse opal hydrogel microparticles were obtained. After the drug was loaded into the microparticles, confocal laser scanning showed FITC-dextran-derived green fluorescence throughout the microparticles

(Figure S5). The dextran drug was uniformly encapsulated in the particles. From Figure 4A, it was found that the dextran was uniformly encapsulated in the particles. Figure 4B shows the fluorescence images of the FITC-dextran loaded inverse opal microparticles under NIR irradiation. The microcarriers shrank because of the photothermal response and the intrinsic fluorescence intensity of FITC-dextran in the microparticles gradually decreased at the same time, indicating drug release.

Notably, characteristic reflection peaks and vivid structural colors resulted from the PBG property of the inverse opal microparticles. Bragg's equation was used to estimate the main peak position λ of the microparticles:

$$\lambda=1.633dn_{average}$$

In which d represents the center-to-center distance between two neighboring nanopores and $n_{average}$ represents the average refractive index of the hydrogel microparticles. Therefore, microparticle shrinkage under NIR irradiation would cause the distance between the nanopores to decrease. Thus, the diffraction-peak positions and colors of the microparticles would change simultaneously. This feature of the microparticles, along with NIR triggered drug release, provides an important ability to self-report drug release levels.

The concentration of calcium alginate would affect the rate of drug release; therefore, we investigated the relationship between the position of the reflection peak at different concentrations of calcium alginate and the amount of released drug at room temperature to select the appropriate encapsulation concentration of calcium alginate. The OD values of the microparticles were obtained using Image J based on the fluorescent images; therefore, the relative release rate could be calculated through the changes of the

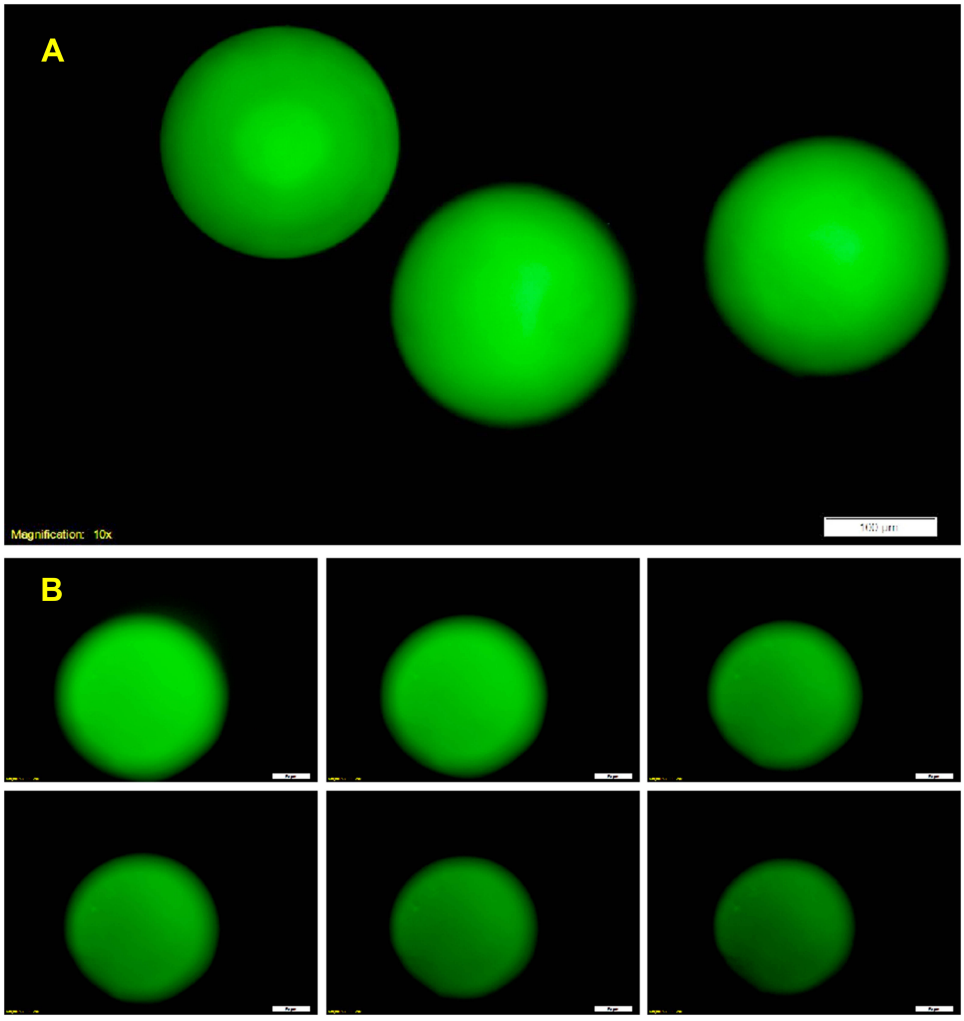

Figure 4 (**A**) Fluorescence image of inverse opal microparticles loaded with fluorescein isothiocyanate (FITC)-dextran. (**B**) In vitro microparticle-released FITC-dextran. In vitro release of the FITC-dextran from the particles, the pictures were captured after drug encapsulating and releasing at a power of 2.5 near-infrared irradiation at 1, 2, 3, 4, 5 and 6 min, the encapsulated calcium alginate hydrogel concentration was 0.2% (w/v). Scale bars are 100 μm in (**A**) and 50 μm in (**B**).

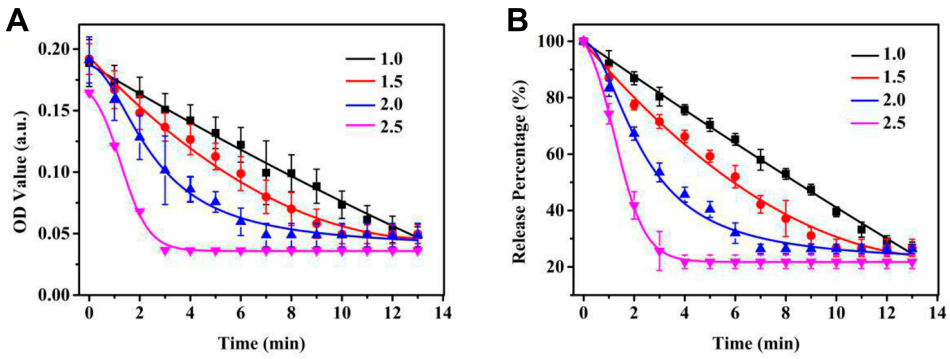

Figure 5 (**A**) Graphs showing the optical density (OD) values of fluorescein isothiocyanate (FITC)-dextran loaded microparticles during the release process under different near-infrared (NIR) irradiation powers (1.0–2.5) (n = 3). (**B**) The release percentage curves of FITC-dextran loaded microparticles under different NIR irradiation powers (1.0–2.5) (n = 3).

OD values. As the calcium alginate concentration increased, the packaging efficiency was enhanced, the cumulative release of the drug decreased, and the release speed decreased (Figure S6a). Therefore, using different calcium alginate concentrations to load drug molecules would permit regulation of the packaging efficiency and the natural release rate of the drug. As shown in (Figure S6b), microcarriers with a high calcium alginate concentration had a low drug release rate. We chose 0.2% calcium alginate hydrogel as the encapsulation concentration for subsequent experiments.

Next, the drug release kinetics in the PBS buffer were recorded under different NIR irradiation levels to determine the drug delivery performance of the FITC-dextran loaded microparticles. The change in the fluorescence of the microparticles was used to calculate the relative drug release (Figure S7). When the NIR power was below 1.0, it took 8 minutes to reach a drug release level of 50% (Figure 5). Increasing NIR power accelerated the drug release rate. When the NIR power was above 2.5, it took only 2 minutes to reach a drug release level of 50%. The relative drug release rate is as well as the reported literature.[49,50] Thus, to achieve the desired result, the release rate of the loaded drugs could be altered using different NIR power levels.

We then used dextran-loaded microparticles with an initial reflection peak of 650 nm to demonstrate their self-reporting feature. Under NIR irradiation, the microparticles gradually contracted. When the microparticles stopped contracting, the NIR source was turned off and the microparticles slowly swelled back to their original state. During this process, we recorded the reflection peaks of the microparticles and the drug release level. Before NIR irradiation, the microparticles had a reflection peak at 650 nm and showed a shiny red structural color. With an increasing duration of NIR irradiation, the microparticles gradually shrank, the reflection peak shifted toward blue and the structural color changed from red to orange, yellow, green, cyan, and blue successively (Figure 6A). The fluorescence intensity of the microparticles decreased along with this blue shift. Figure 6B shows the relationship between the release level and the reflection images. The amount of drug released could be

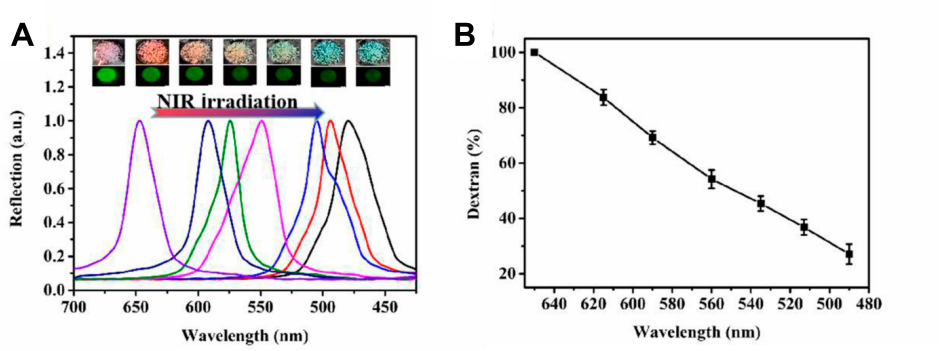

Figure 6 (**A**) Drug-loaded inverse opal microparticles' reflection spectra, reflection images, and fluorescence images under near-infrared (NIR) irradiation; (**B**) The relationship between the drug release level and the reflection peak positions (n = 3).

estimated quantitatively used the structural color or the reflection peak position. For example, at a reflection peak of 615 nm, the drug release rate was 16% and the microcarriers were orange. While at a reflection peak of 535 nm, the drug release rate was 55% and the microcarriers were green. Drug release from the inverse opal microparticle-based drug delivery system could be monitored visually, which simplified the use of detection instruments and procedures.

Conclusion

In the present study, a novel drug delivery system with self-reporting controllable release was developed. Microparticles comprising GO/pNIPAM/PEGDA composite hydrogel inverse opal scaffolds, with dextran and calcium alginate hydrogel were synthesized using SCCBs as the template. The photothermal phase transition behavior release function under NIR irradiation. Moreover, the high refractive index of PEGDA allows real-time drug release monitoring, with the color of the microcarriers as the signal. Compared with other particle-based delivery systems, our system saves monitoring time in terms of instrumentation and allows easier controlled drug release. During external drug delivery applications, the practical application of the NIR exposure time and the antibacterial properties of the microparticles will be further studied. We predict that the developed method will promote new pathways of drug discovery and development. The responsive performances of the developed microparticles markedly widen the functions and applications of particle delivery systems for drug delivery and development.

Acknowledgments

This work was supported by the "Double First-Class" University Project [grant number CPU2018GY25]. The funding source had no role in study design; in the collection, analysis and interpretation of data; in the writing of the report; or in the decision to submit the article for publication.

Disclosure

Xiaoyan Sun, Hui Zou, Caixia Yao and Baofen Ye report an issued patent: CN201910226335.8 (Applicant (patent right): China Pharmaceutical University; Preparation method and application of controlled release microsphere carrier capable of visual monitoring; Application date: 2019.06.21). The authors report no other possible conflicts of interest in this work.

References

1. Fonte P, Reis S, Sarmento B. Facts and evidences on the lyophilization of polymeric nanoparticles for drug delivery. *J Control Release*. 2016;225:75–86. doi:10.1016/j.jconrel.2016.01.034
2. Bhise NS, Ribas J, Manoharan V, et al. Organ-on-a-chip platforms for studying drug delivery systems. *J Control Release*. 2014;190:82–93. doi:10.1016/j.jconrel.2014.05.004
3. Rodkate N, Rutnakornpituk M. Multi-responsive magnetic microsphere of poly(N-isopropylacrylamide)/carboxymethylchitosan hydrogel for drug controlled release. *Carbohydr Polym*. 2016;151:251–259. doi:10.1016/j.carbpol.2016.05.081
4. Kim H, Lee H, Seong K-Y, Lee E, Yang SY, Yoon J. Visible light-triggered on-demand drug release from hybrid hydrogels and its application in transdermal patches. *Adv Healthc Mater*. 2015;4(14):2071–2077. doi:10.1002/adhm.201500323
5. Yang X, He D, He X, et al. Synthesis of hollow mesoporous silica nanorods with controllable aspect ratios for intracellular triggered drug release in cancer cells. *ACS Appl Mater Interfaces*. 2016;8(32):20558–20569. doi:10.1021/acsami.6b05065
6. Chen C, Liu Y, Sun L, et al. Antibacterial porous microcarriers with a pathological state responsive switch for wound healing. *ACS Appl Bio Mater*. 2019;2(5):2155–2161. doi:10.1021/acsabm.9b00134
7. Patel M, Moon HJ, Ko Du Y, Jeong B. Composite system of graphene oxide and polypeptide thermogel as an injectable 3D scaffold for adipogenic differentiation of tonsil-derived mesenchymal stem cells. *ACS Appl Mater Interfaces*. 2016;8(8):5160–5169. doi:10.1021/acsami.5b12324
8. Cai B, Zhao M, Ma Y, Ye Z, Huang J. Bioinspired formation of 3D hierarchical CoFe2O4 porous microspheres for magnetic-controlled drug release. *ACS Appl Mater Interfaces*. 2015;7(2):1327–1333. doi:10.1021/am507689a
9. Shirakura T, Kelson TJ, Ray A, Malyarenko AE, Kopelman R. Hydrogel nanoparticles with thermally controlled drug release. *ACS Macro Lett*. 2014;20143(7):602–606. doi:10.1021/mz500231e
10. Li J, Wang Y, Zhang L, Xu Z, Dai H, Wu W. Nanocellulose/gelatin composite cryogels for controlled drug release. *ACS Sustain Chem Eng*. 2019;7(6):6381–6389. doi:10.1021/acssuschemeng.9b00161
11. Qiu M, Wang D, Liang W, Liu L, Zhang Y. Novel concept of the smart NIR-light-controlled drug release of black phosphorus nanostructure for cancer therapy. *PNAS*. 2018;115(3):1–6. doi:10.1073/pnas.1714421115
12. Ji X, Kong N, Wang J, Li W, Xiao Y. A novel top-down synthesis of ultrathin 2D boron nanosheets for multimodal imaging-guided cancer therapy. *Adv Mater*. 2018;30(36):1803031–1803041. doi:10.1002/adma.201803031
13. Xing C, Chen S, Liang X, Liu Q, Qu X. Two-dimensional MXene (Ti3C2)- integrated cellulose hydrogels: toward smart three-dimensional network nanoplatforms exhibiting light-induced swelling and bimodal photothermal/chemotherapy anticancer activity. *ACS Appl Mater Interfaces*. 2018;10:27631–27643. doi:10.1021/acsami.8b08314
14. Tao W, Ji X, Zhu X, Li L, Wang J, Zhang Y. Two-dimensional antimonene-based photonic nanomedicine for cancer theranostics. *Adv Mater*. 2018;30(38):1802061–1802071. doi:10.1002/adma.201802061
15. Sun Z, Zhao Y, Li Z, Cui H, Zhou Y, Li W. TiL4-coordinated black phosphorus quantum dots as an efficient contrast agent for in vivo photoacoustic imaging of cancer. *Small*. 2017;13(11):1602896–-1602902. doi:10.1002/smll.201602896
16. Tao W, Ji X, Xu X, Mohammad AI, Li Z. Antimonene quantum dots: synthesis and application as near-infrared photothermal agents for effective cancer therapy. *Angewandte Chemie*. 2017;56(39):11896–11900. doi:10.1002/anie.201703657
17. Xing C, Chen S, Qiu M, Liang X, Liu Q, Zou Q. Conceptually novel black phosphorus/cellulose hydrogels as promising photothermal agents for effective cancer therapy. *Adv Healthc Mater*. 2018;7(7):1701510–1701520. doi:10.1002/adhm.201701510

18. Sharma M, Waterhouse GI, Loader SW, Garg S, Svirskis D. High surface area polypyrrole scaffolds for tunable drug delivery. *Int J Pharm*. 2013;443(1–2):163–168. doi:10.1016/j.ijpharm.2013.01.006
19. Wang Y, Shang L, Chen G, et al. Pollen-inspired microparticles with strong adhesion for drug delivery. *Appl Mater Today*. 2018;13:303–309. doi:10.1016/j.apmt.2018.09.016
20. Jiao X, Li Y, Li F, et al. pH-responsive nano sensing valve with self-monitoring state property based on hydrophobicity switching. *RSC Adv*. 2016;6:52292–52299. doi:10.1039/c6ra08948h
21. Zhao M, Wu W, Su B. pH-controlled drug release by diffusion through silica nanochannel membranes. *ACS Appl Mater Interfaces*. 2018;10(40):33986–33992. doi:10.1021/acsami.8b12200
22. Kim D, Jo A, Imani KBC, Kim D, Chung JW, Yoon J. Microfluidic fabrication of multistimuli-responsive tubular hydrogels for cellular scaffolds. *Langmuir*. 2018;34(14):4351–4359. doi:10.1021/acs.langmuir.8b00453
23. Son KH, Lee JW. Synthesis and characterization of poly(ethylene glycol) based thermo-responsive hydrogels for cell sheet engineering. *Materials (Basel)*. 2016;9(10). doi:10.3390/ma9100854
24. He D, He X, Wang K, Zou Z, Yang X, Li X. Remote-controlled drug release from graphene oxide-capped mesoporous silica to cancer cells by photoinduced pH-jump activation. *Langmuir*. 2014;30(24):7182–7189. doi:10.1021/la501075c
25. Xu Y, Wang H, Luan C, Liu Y, Chen B, Zhao Y. Aptamer-based hydrogel barcodes for the capture and detection of multiple types of pathogenic bacteria. *Biosens Bioelectron*. 2018;100:404–410. doi:10.1016/j.bios.2017.09.032
26. Amini-Fazl MS, Mohammadi R, Kheiri K. 5-Fluorouracil loaded chitosan/polyacrylic acid/Fe3O4 magnetic nanocomposite hydrogel as a potential anticancer drug delivery system. *Int J Biol Macromol*. 2019;132:506–513. doi:10.1016/j.ijbiomac.2019.04.005
27. Seyfoddin A, Chan A, Chen WT, Rupenthal ID, Waterhouse GI, Svirskis D. Electro-responsive macroporous polypyrrole scaffolds for triggered dexamethasone delivery. *Eur J Pharm Biopharm*. 2015;94:419–426. doi:10.1016/j.ejpb.2015.06.018
28. Cheon YA, Bae JH, Chung BG. Reduced graphene oxide nanosheet for chemo-photothermal therapy. *Langmuir*. 2016;32(11):2731–2736. doi:10.1021/acs.langmuir.6b00315
29. Tao W, Kong N, Ji X, Zhang Y. Emerging two-dimensional monoelemental materials (Xenes) for biomedical applications. *Chem Soc Rev*. 2019;48:2891–2912. doi:10.1039/c8cs00823j
30. Luo M, Fan T, Zhou Y, Zhang H, Mei L. 2D black phosphorus-based biomedical applications. *Adv Funct Mater*. 2019;29(13):1808306–-1808324. doi:10.1002/adfm.201808306
31. Qiu M, Ajay S, Wang D, Junle Q, Mark S, Zhang H. Biocompatible and biodegradable inorganic nanostructures for nanomedicine: silicon and black phosphorus. *Nano Today*. 2019;25:135–155. doi:10.1016/j.nantod.2019.02.012
32. Shang L, Wang Y, Yu Y, et al. Bio-inspired stimuli-responsive graphene oxide fibers from microfluidics. *J Mater Chem A*. 2017;5(29):15026–15030. doi:10.1039/c7ta02924a
33. Zhao Z, Wang H, Shang L, et al. Bioinspired heterogeneous structural color stripes from capillaries. *Adv Mater*. 2017;29(46):1704569. doi:10.1002/adma.201704569
34. Liu C, Liu X, Xuan H, Ren J, Ge L. A smart colorful supercapacitor with one dimensional photonic crystals. *Sci Rep*. 2015;5:18419. doi:10.1038/srep18419
35. Ren J, Xuan H, Liu C, et al. Graphene oxide hydrogel improved sensitivity in one-dimensional photonic crystals for detection of beta-glucan. *RSC Adv*. 2015;5(94):77211–77216. doi:10.1039/c5ra12155h
36. Wang P, Huang C, Xing Y, et al. NIR-light- and pH-responsive graphene oxide hybrid cyclodextrin-based supramolecular hydrogels. *Langmuir*. 2019;35(4):1021–1031. doi:10.1021/acs.langmuir.8b03689
37. Bardajee GR, Hooshyar Z, Farsi M, Mobini A, Sang G. Synthesis of a novel thermo/pH sensitive nanogel based on salep modified graphene oxide for drug release. *Mater Sci Eng C*. 2017;72:558–565. doi:10.1016/j.msec.2016.11.109
38. Ding C, Tong L, Feng J, Fu J. Recent advances in stimuli-responsive release function drug delivery systems for tumor treatment. *Molecules*. 2016;21(12):1715. doi:10.3390/molecules21121715
39. Cai W, Wang J, Chu C, Chen W, Wu C, Liu G. Metal-organic framework-based stimuli-responsive systems for drug delivery. *Adv Sci*. 2019;6:1801526. doi:10.1002/advs.201801526
40. Liu C, Ding H, Wu Z, et al. Tunable structural color surfaces with visually self-reporting wettability. *Adv Funct Mater*. 2016;26(43):7937–7942. doi:10.1002/adfm.201602935
41. Ding H, Zhu C, Tian L, et al. Structural color patterns by electrohydrodynamic jet printed photonic crystals. *ACS Appl Mater Interfaces*. 2017;9(13):11933–11941. doi:10.1021/acsami.6b11409
42. Hou J, Li M, Song Y. Recent advances in colloidal photonic crystal sensors: materials, structures and analysis methods. *Nano Today*. 2018;22:132–144. doi:10.1016/j.nantod.2018.08.008
43. Wen L, Hou X, Tian Y, et al. Bioinspired smart gating of nanochannels toward photoelectric-conversion systems. *Adv Mater*. 2010;22(9):1021–1024. doi:10.1002/adma.200903161
44. Shang Y, Chen Z, Fu F, et al. Cardiomyocyte-driven structural color actuation in anisotropic inverse opals. *ACS Nano*. 2018;13(1):796–802. doi:10.1021/acsnano.8b08230
45. Kim JB, Lee SY, Lee JM, Kim S-H. Designing structural-color patterns composed of colloidal arrays. *ACS Appl Mater Interfaces*. 2019;11(16):14485–14509. doi:10.1021/acsami.8b21276
46. Xu Q, Wang H, Fu F, Liu C, Chen Z, Zhao Y. Cuttlefish ink tagged photonic crystal particles and their ion-responsive construction. *J Nanosci Nanotechnol*. 2018;18(7):4834–4840. doi:10.1166/jnn.2018.15346
47. Fu F, Chen Z, Zhao Z, et al. Bio-inspired self-healing structural color hydrogel. *Proc Natl Acad Sci U S A*. 2017;114(23):5900–5905. doi:10.1073/pnas.1703616114
48. Chen C, Liu Y, Wang H, et al. Multifunctional chitosan inverse opal particles for wound healing. *ACS Nano*. 2018;12(10):10493–10500. doi:10.1021/acsnano.8b06237
49. Zhang B, Cheng Y, Wang H, et al. Multifunctional inverse opal particles for drug delivery and monitoring. *Nanoscale*. 2015;7(24):10590–10594. doi:10.1039/c5nr02324f
50. Liu Y, Shao C, Bian F, Yu Y, Wang H, Zhao Y. Egg components composited inverse opal particles for synergistic drug delivery. *ACS Appl Mater Interfaces*. 2018;10(20):17058–17064. doi:10.1021/acsami.8b03483